ResearchGate

See discussions, stats, and author profiles for this publication at: https://www.researchgate.net/publication/281225901

Double Perovskite LaSrCo1.6Cu0.4O5- Cathode for IT-SOFCs with Pulsed Laser Technique Deposited Bi-Layer...

Article *in* Journal of The Electrochemical Society · July 2015

DOI: 10.1149/2.0851509jes

CITATION
1

READS
11

5 authors, including:

Yen-Pei Fu
National Dong Hwa University
139 PUBLICATIONS **1,673** CITATIONS
SEE PROFILE

Adi Subardi
National Dong Hwa University
8 PUBLICATIONS **19** CITATIONS
SEE PROFILE

All content following this page was uploaded by Yen-Pei Fu on 20 April 2017.

The user has requested enhancement of the downloaded file.

Journal of The Electrochemical Society, **162** (9) F1029-F1035 (2015)
0013-4651/2015/162(9)/F1029/7/$33.00 © The Electrochemical Society

Double Perovskite $LaSrCo_{1.6}Cu_{0.4}O_{5-\delta}$ Cathode for IT-SOFCs with Pulsed Laser Technique Deposited Bi-Layer Electrolyte

Yen-Pei Fu,[z] Rou-Hua Chen, Min-Yen Hsieh, Adi Subardi, and Wen-Ku Chang

Department of Materials Science and Engineering, National Dong Hwa University Shou-Feng, Hualien 97401, Taiwan

This study included two parts: (1) the structural characteristics, chemical stability, thermal expansion coefficient (TEC), chemical bulk diffusion coefficient (D_{chem}), chemical surface exchange coefficient (k_{chem}), electrochemical performance and single cell performance for $LaSrCo_{1.6}Cu_{0.4}O_{5+\delta}$ as an intermediate-temperature solid oxide fuel cells (IT-SOFC) cathode material, and (2) using a pulsed laser technique (PLD) deposited a dense $Ce_{0.8}Sm_{0.2}O_{1.9}$ (SDC) thin layer on thick SDC as bi-layer electrolyte and infiltrating SDC nanoparticles onto $LaSrCo_{1.6}Cu_{0.4}O_{5+\delta}$ skeleton to improve the performance of the single cell. The single cell assembling with 0.5M SDC-infiltrated $LaSrCo_{1.6}Cu_{0.4}O_{5+\delta}$ cathode and PLD-deposited SDC/SDC bilayer have shown very good performance at low operating temperatures.
© 2015 The Electrochemical Society. [DOI: 10.1149/2.0851509jes] All rights reserved.

Manuscript submitted May 8, 2015; revised manuscript received June 16, 2015. Published July 1, 2015.

Currently, solid oxide fuel cells (SOFCs) have attracted a great deal of attention due to the advantages of high electrical efficiency, fuel versatility, low-pollutant emission, etc.[1–3] However, a high operating temperatures limits the application of SOFCs and lowers operating temperature to around 600°C is primary goal in current SOFC research. Lately, research efforts have been devoted to decreasing a high operating temperature. Electrolyte materials with high ionic conductivity, such as Samaria-doped ceria (SDC),[4] bismuth oxides,[5] and lanthanum strontium gallate magnesite (LSGM)[6] have received attention for intermediate temperature SOFCs. SDC is considered one of the most promising materials for SOFCs. Its conductivity is 2–3 times greater than that of yttria stabilized zirconia (YSZ).[7] Nevertheless, one main limitation of the SDC electrolyte is the reduction of Ce^{4+} to Ce^{3+} induces n-type electronic conduction, which tends to decrease the open circuit voltage (OCV) and a consequent decrease in the overall power output.[8–11] The problem can be eliminated by incorporating dense and thin SDC on surface of thick SDC electrolyte as a blocking layer to improve the stability of the SDC electrolyte under the reducing environment and inhibit electronic current leakage. The pulsed laser deposition (PLD) technique is a promising method that offers better control of the deposited film properties, such as microstructures, density and stoichiometric with multi-component materials.[12,13] Furthermore, the PLD technique can operate at a low processing temperature without high post-annealing temperature,[14] which is useful for low temperature SOFC applications. Therefore, we researched lower heating temperature (600°C) for the PLD procedure to fabricate dense and thin SDC layers on thick SDC electrolytes prepared by a solid-state reaction. In this paper, we used a simpler approach that uses a highly conductive and chemically stable on conductor electrolyte was developed by protecting a sintered SDC pellet with a thin SDC layer. The overall performance of the bilayer electrolyte turned out to be of great interest. The bilayer electrolyte was fabricated using a 1 mm thick pellet of anode-supported SDC as a substrate and about a 0.1 μm SDC film grown on it by PLD technique (Fig. 1).

Potential cathode candidates normally is based on mixed oxygen ionic and electronic conducting oxides with high electrocatalytic activity for oxygen reduction reaction (ORR).[15–19] The mixed ionic and electronic conductor (MIEC) extends the active oxygen reduction sites from the typical electrolyte-electrode-gas triple-phase boundary to the entire cathode surface, which leads to greatly reduced the cathode polarization at low operating temperatures.[20] Therefore, seeking cathode materials with high electrocatalytic activity for oxygen reduction reactions at intermediate temperatures is of great importance and has received considerable attention in the past decade. Among MIECs, the research has focused on $LnBaM'M''O_{5+\delta}$ layered perovskite oxides, wherein the B-site is occupied by equal amount of different 3d transition metal cations (M′, M″ = Mn, Fe, Co, Ni, Cu). This is due to a much higher chemical diffusion and surface exchange coefficients relative to those of ABO_3-type perovskite oxides.[21] Further, the oxygen-deficient double-perovskites $LnBaCo_2O_{5+\delta}$ (Ln = La, Pr, Nd, Sm, Gd, Y, etc.), have received a great deal of attention for their potential applications in intermediate-temperature solid oxide fuel cells (IT-SOFCs).[22,23] These double perovskites possess an ordered structure that consists of alternating lanthanide and alkali-earth planes along the c-axis as described in the following stacking sequence $[LnO_\delta]$-$[CoO_2]$-[BaO]-$[CoO_2]$, whereas the oxygen vacancies are primarily located in the rare-earth planes $[LnO_\delta]$.[24,25] Mixed ionic-electronic conductors (MIECs) containing Mn, Fe, Ni, and Cu have demonstrated excellent catalytic performance under intermediate operating temperature conditions. However, cobalt-containing cathodes encounter problems such as high thermal expansion coefficients and poor stability as well as the high cost of cobalt. Significant efforts have been devoted to optimizing catalytic activity of perovskite oxides through various ion substitutions to solve these problems of cobalt containing cathode and to achieve better cell performance at relatively low temperatures.[26–28] Partial substation of other elements for cobalt in cobalt-containing cathodes are considered a possible means to compensate for its disadvantages.[29]

The oxygen reduction reaction (ORR) activity of a SOFC cathode is closely related to the surface exchange and oxygen bulk diffusion properties. Detailed information about these properties is useful to understand the electrochemical properties necessary to perform as a cathode and provide further guidance for performance optimization.[30] The electrical conductivity relaxation (ECR) method is a simple approach to measure the chemical bulk diffusion coefficient (D_{chem}) and chemical surface exchange coefficient (k_{chem}) of a mixed conductor due to the high sensitivity of the electrical conductivity changes in various oxygen concentrations or oxygen partial pressures.[31–34] This approach was used to evaluate the chemical bulk diffusion coefficients (D_{chem}) and chemical surface exchange coefficient (k_{chem}) of $LaSrCo_{1.6}Cu_{0.4}O_{5+\delta}$ cathode.

A common approach is depositing active ionic-conductive nano-sized particles on a porous cathode skeleton using an infiltration or impregnation technique to improve cathode performance, which could provide a larger number of oxygen reduction reaction sites and improve the electrochemical performance, resulting in relatively low area specific resistances.[35–39] In this study, the transition element of Cu was incorporated into the layered perovskite $LaSrCo_2O_{5+\delta}$ to search the high performance cathode for IT-SOFCs, $LaSrCo_{1.6}Cu_{0.4}O_{5+\delta}$ cathode was infiltrated with nano-sized $Ce_{0.8}Sm_{0.2}O_{1.9}$ electrolyte particles to improve cathode performance and the anode-supported single fuel cell with pulsed laser deposited bi-layer $Ce_{0.8}Sm_{0.2}O_{1.9}$ electrolyte was set up to measure current-voltage curves and evaluate performances.

Experimental

A conventional solid-state reaction synthesis method was applied to prepare $LaSrCo_{1.6}Cu_{0.4}O_{5-\delta}$ (LSCO-Cu) cathode powder. The

[z]E-mail: d887503@alumni.nthu.edu.tw

Downloaded on 2015-07-15 to IP 134.208.4.209 address. Redistribution subject to ECS terms of use (see ecsdl.org/site/terms_use) unless CC License in place (see abstract).

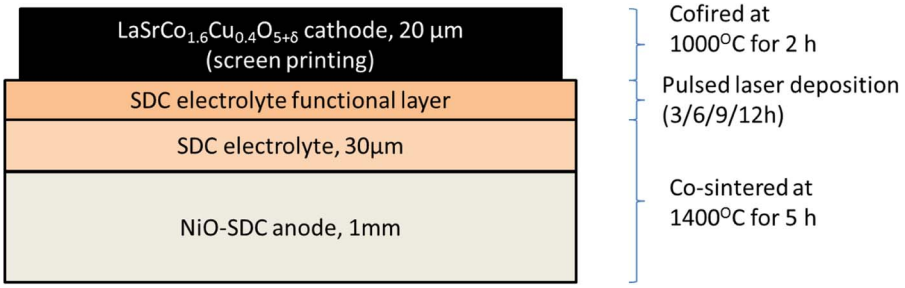

Figure 1. A schematic drawing of the cell structure and its fabrication method.

ball-milled mixture was dried and ground into a powder with mortar and pestle and then calcined in air at 900°C for 4 h. The LSCO-Cu cathode bulk material was prepared to assess its bulk diffusion properties. The cathode powder was pelletized with a small amount of PVA as a binder with an applied uniaxial pressure of 1000 kgf cm^{-2}, and then the calcined cathode was air sintered at 1100°C for 4 h with a programmed heating rate of 5°C min^{-1} to measure the oxygen bulk diffusion properties. The $Ce_{0.8}Sm_{0.2}O_{1.9}$ (SDC) powder was synthesized by coprecipitation and calcined at 600°C for 2 h.[40] The structure of $LaSrCo_{1.6}Cu_{0.4}O_{5-\delta}$ was characterized by X-ray powder diffractometer (XRD; Rigaku D/MAX-2500 V) by a scanning rate of 4° min^{-1} and a scanning range of 20–80° using a Cu K_α(1.5418 Å) radiation source. The powder pattern and lattice parameters were analyzed by Rietveld refinement using the GSAS program. In order to investigate the chemical stability between LSCO-Cu cathode and SDC phase, the mixture powder of 50 wt% LSCO-Cu cathode + 50 wt% SDC were mixed under ethanol and milled for 12 h using zirconia ball, and then cofired in air from 900°C to 1100°C for 4 h. These mixed powders with heat-treatment were also characterized by X-ray powder diffractometer. The thermal expansion coefficients of the $LaSrCo_2O_{5-\delta}$ and $LaSrCo_{1.6}Cu_{0.4}O_{5-\delta}$ specimens sintered in air at 1100°C were measured using a dilatometer (DIL; Model Netzsch DIL 402 PC, Bavaria, Germany) using a constant heating rate of 10°C min^{-1} in the temperature range of 25–650°C in air.

The time dependence of the conductivity was measured using the four-probe DC technique and was recorded using a Keithley 2420 source meter. The measurement was performed on $LaSrCo_{1.6}Cu_{0.4}O_{5+\delta}$ specimen with rectangular geometry using a typical size of 50 × 1.5 × 1.5 mm^3 and greater than 95% of the theoretical density over the temperature range of 500–700°C at an interval of 50°C. After each temperature change, the bar was stabilized for at least 30 min. A sudden change in the oxygen partial pressure from 0.21 to 0.05 atm was caused by the introduction of standard gas mixtures of Ar and O_2. An oxidation step was performed to investigate the D_{chem}. Typically, a sequence of oxidation curves was obtained at each temperature. The electrical conductivity relaxation curve was plotted as g(t) versus t. The values for D_{chem} and k_{chem} were determined by fitting the electrical conductivity relaxation curves into Equation 1, in which D_{chem}, measured in cm^2/s, and the surface exchange coefficient, k_{chem}, measured in cm/s.[41]

$$\frac{\sigma(t)-\sigma(0)}{\sigma(\infty)-\sigma(0)} = 1 - \sum_{n=1}^{\infty}\sum_{m=1}^{\infty}\sum_{p=1}^{\infty} \times \frac{2C_1^2 \exp\left(-\alpha_{1n}^2 D_{chem} t/l_l^2\right)}{\alpha_{1n}^2\left(\alpha_{1n}^2 + C_1^2 + C_1\right)} \times \frac{2C_2^2 \exp\left(-\alpha_{2m}^2 D_{chem} t/l_2^2\right)}{\alpha_{2m}^2\left(\alpha_{2m}^2 + C_2^2 + C_2\right)} \times \frac{2C_3^2 \exp\left(-\alpha_{3p}^2 D_{chem} t/l_3^2\right)}{\alpha_{3p}^2\left(\alpha_{3p}^2 + C_3^2 + C_3\right)} \quad [1]$$

where σ(0), σ(t), and σ(∞) indicate the initial, time independent and final conductivities, respectively. The coefficients of α_{1n}, α_{2m}, α_{3p} are the nth, mth and pth roots of the transcendental equations:

$$C_1 = \alpha_{1n}\tan\alpha_{1n}, \quad C_2 = \alpha_{2m}\tan\alpha_{2m}, \quad C_3 = \alpha_{3p}\tan\alpha_{3p} \quad [2]$$

The parameters of C_1, C_2, and C_3 are defined as :

$$C_1 = \frac{l_1}{L_d}, \quad C_2 = \frac{l_2}{L_d}, \quad C_3 = \frac{l_3}{L_d}, \quad L_d = \frac{D_{chem}}{k_{ex}} \quad [3]$$

The working electrode (WE), $LaSrCo_{1.6}Cu_{0.4}O_{5+\delta}$ cathode, was prepared on a sintered SDC. The cathode pastes consists of cathode powders, solvent, binder, and plasticizer. The cathode paste was applied on both sides of the sintered SDC electrolyte discs with circle patterns using the screen-printing method with a diameter of 13 mm and a thickness of 1 mm. On a side for each one, the cathode paste was painted as the working electrode (WE) with a surface area of 0.385 cm^2. The Pt reference electrode (RE) was located approximately 0.3–0.4 cm away from the WE. This distance was selected to avoid measurement errors due to the misalignment of the working and counter electrodes. The Pt counter electrode (CE) was arranged on the other side of the sintered SDC disk. After the cathode material was painted on the electrolyte, it was then sintered at 1000°C for 4 h in air. The symmetrical testing-cell experiments were performed over temperatures ranging from 600–850°C at intervals of 50°C in a furnace under air (P_{O_2} = 0.21atm). The applied frequency range of the AC impedance measurements using a VoltaLab PGZ301 potentiostat ranged from 100 kHz to 0.1 Hz with a 10-mV AC signal amplitude. The electrochemical impedance spectroscopy (EIS) fitting analysis was performed using Zview.

Anode-supported fuel cells were fabricated to evaluate the performance of a single cell with a SDC electrolyte (30 μm), a dense PLD-deposited SDC thin film, a NiO+SDC anode (1 mm), and a LSCO-Cu cathode (20 μm). The SDC powders and NiO-SDC substrate were co-pressed to form a green SDC electrolyte/NiO-SDC anode bilayer. They were subsequently co-sintered at 1400°C for 4 h. The PLD-deposited SDC electrolyte was fabricated by a SDC target fabricated by coprecipitation process and sintered at 1500°C for 5 h with a KrF excimer laser at a repetition rate of 10 Hz. A dense SDC thin layer was deposited by PLD on the SDC electrolyte/NiO-SDC anode substrate to form PLD-deposited SDC/SDC/NiO-SDC configuration. The LSCO-Cu cathode paste was screen-printed onto PLD-deposited SDC/SDC/NiO-SDC and cofired at 1000°C for 4 h. Figure 1 shows a schematic drawing of the cell structure and its fabrication methods. 3μL of 0.5 M SDC precursor was infiltrated into LSCO-Cu cathode backbones to obtain high performance of a single cell. Finally, the infiltration cell was fired at 900°C for 2 h to obtain the desired SDC phase dispersed on the LSCO-Cu backbones. The button cell with an effective area of 0.316 cm^2 was measured with humidified hydrogen (50 mL min^{-1}, 3 vol% H_2O) as fuel and air (100 mL min^{-1}) as oxidants to evaluate the performance of the fabricated anode-supported solid oxide fuel cells. The current-voltage characteristics of the single cells were measured in a temperature range of 500–800°C at intervals of 100°C.

Results and Discussion

The Rietveld refinement of $LaSrCo_{1.6}Cu_{0.4}O_{5+\delta}$ include the measured XRD pattern and the calculated profile. Figure 2 shows the difference between them. There is an excellent agreement between the experimental data and the calculated profiles, which exhibits cations that are well ordered between La^{3+}/Sr^{2+} and $Co^{3+/}Cu^{2+}$ ions in an

Downloaded on 2015-07-15 to IP 134.208.4.209 address. Redistribution subject to ECS terms of use (see ecsdl.org/site/terms_use) unless CC License in place (see abstract).

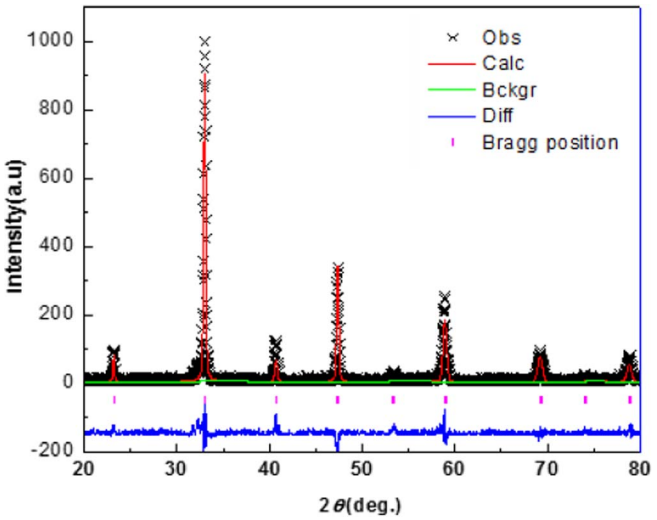

Figure 2. X-ray powder diffraction pattern and Rietveld refinement of $LaSrCo_{1.6}Cu_{0.4}O_{5+\delta}$ calcined at 1000°C. Observed (crosses) and calculated (solid line) XRD profiles, and the difference (bottom line) between them.

ordered perovskite lattice. Table I lists the Rietveld refinement data and reveals the diffraction pattern of $LaSrCo_{1.6}Cu_{0.4}O_{5+\delta}$ samples could be indexed to a cubic structure (space group: $Pm\bar{3}\,m$) with lattice parameter, a = 3.838 Å, b = 3.838 Å and c = 3.838 Å. Figure 3 shows the XRD patterns of 50 wt% LSCO-Cu cathode + 50 wt% SDC electrolyte calcined at various temperatures for 4 h. LSCO-Cu contains a perovskite structure, while SDC contains a cubic fluorite-type structure, they are different structures. This reveals that no obvious interface reaction appeared for 50 wt% LSCO-Cu cathode + 50 wt% SDC electrolyte composites heated up to 1000°C for 4 h (Fig. 3a and 3b) as based on chemical stability results; whereas, there are secondary phases that appeared during the test of chemical stability (Fig. 3c). This suggests that a certain degree of solid-state reaction might have occurred between the LSCO-Cu and SDC phases at 1100°C. Therefore, LSCO-Cu is a chemically stable cathode for a SDC electrolyte based SOFC when the cofired temperature is less than 1100°C. We refer a cofired temperature of 1000°C to assemble single cells in future works.

A bulk thermal expansion study on $LaSrCo_2O_{5+\delta}$, $LaSrCo_{1.6}Cu_{0.4}O_{5+\delta}$ cathodes and $Ce_{0.8}Sm_{0.2}O_{1.9}$ electrolyte was conducted from room temperature to 600°C using a dilatometer in air (Fig. 4). Table II lists the detailed information regarding thermal expansion. The larger TEC values of cobalt-based perovskite oxides can be mainly ascribed to two reasons: (1) the reduction of smaller Co^{4+} to larger Co^{3+} with a loss of oxygen and (2) Co^{3+} ions easily transit from low-spin to high spin with increasing temperature.[42–44] Clearly, doping Cu elements into B-site of layered LSCO perovskite cathode reduced their thermal expansion coefficients. The thermal expansion curves deviated from linearity in some degrees as shown

Table I. Crystal structure of $LaSrCo_{1.6}Cu_{0.4}O_{5+\delta}$ cell parameters obtained from the Rietveld refinement.*

Atom	X	Y	Z	Uiso	Occup
La1	0.5	0.5	0.5	0.02344	0.3827
Sr2	0.5	0.5	0.5	0.72915	0.1709
Co3	0	0	0	0.00529	0.6987
Cu4	0	0	0	0.00508	0.1824
O5	0.5	0.5	0	0.04098	0.9054

*Space group $Pm\bar{3}m$ cubic structure, a = 3.838 Å, b = 3.838 Å, c = 3.838 Å, R_p = 1.87%, R_{wp} = 2.89%, χ^2 = 3.06

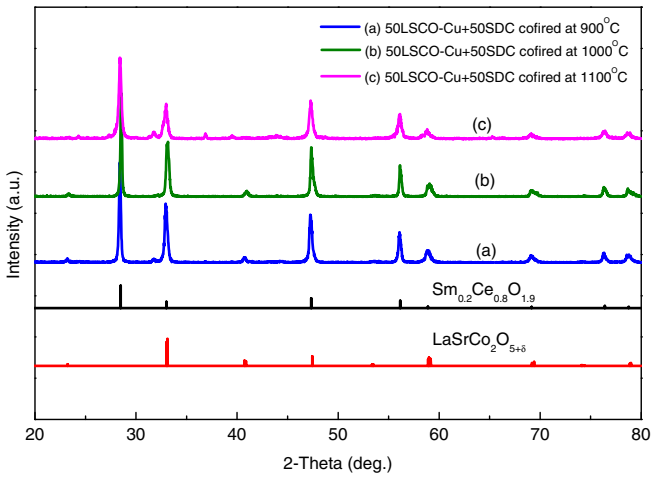

Figure 3. X-ray diffraction patterns of the powder mixture of 50 wt% $LaSrCo_{1.6}Cu_{0.4}O_{5+\delta}$ cathode +50 wt% $Ce_{0.8}Sm_{0.2}O_{1.9}$ electrolyte calcined at (a) 900°C, (b)1000°C and (c) 1100°C, respectively for 4 h.

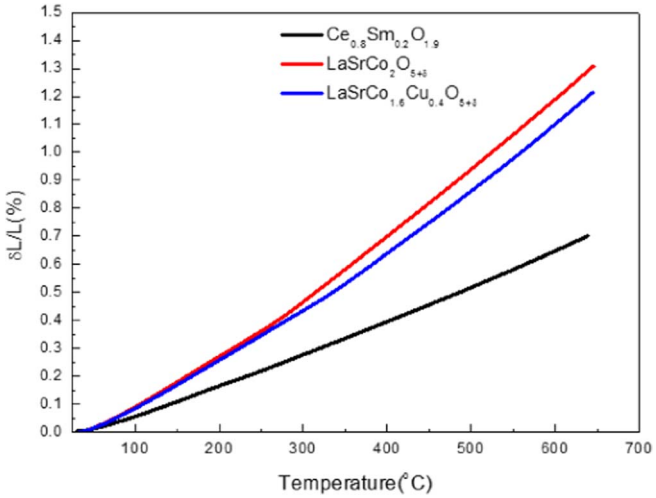

Figure 4. Thermal expansions of $LaSrCo_2O_{5+\delta}$, $LaSrCo_{1.6}Cu_{0.4}O_{5+\delta}$ cathodes, and $Ce_{0.8}Sm_{0.2}O_{1.9}$ electrolyte as a function of temperature over the temperature range of 30–600°C.

in LSCO and LSCO-Cu cathodes at approximately 300°C, which temperature is not associated with a phase transition. Based on our previous studies,[45] the high temperature lattice expansion is associated with the loss of lattice oxygen. The formation of oxygen vacancies may be ascribed to the following results: (1) the repulsion force arising between those mutually exposed cations when oxygen ions are extracted from the lattice; and (2) the increase in cation size due to the reduction of the Co ions from Co^{3+} to Co^{2+} valences, which must occur concurrently with the creation of oxygen vacancies in order to maintain electrical neutrality.[46]

Cathode performance is strongly related to the intrinsic properties of the materials, such as the bulk diffusion and surface exchange

Table II. Thermal expansion coefficients of $LaSrCo_2O_{5+\delta}$, $LaSrCo_{1.6}Cu_{0.4}O_{5+\delta}$ cathodes and $Ce_{0.8}Sm_{0.2}O_{1.9}$ electrolyte over the temperature range of 25–650°C.

Specimens	TEC (ppm K^{-1})
$LaSrCo_2O_{5+\delta}$	21.37
$LaSrCo_{1.6}Cu_{0.4}O_{5+\delta}$	19.75
$Ce_{0.8}Sm_{0.2}O_{1.9}$	12.37

Downloaded on 2015-07-15 to IP 134.208.4.209 address. Redistribution subject to ECS terms of use (see ecsdl.org/site/terms_use) unless CC License in place (see abstract).

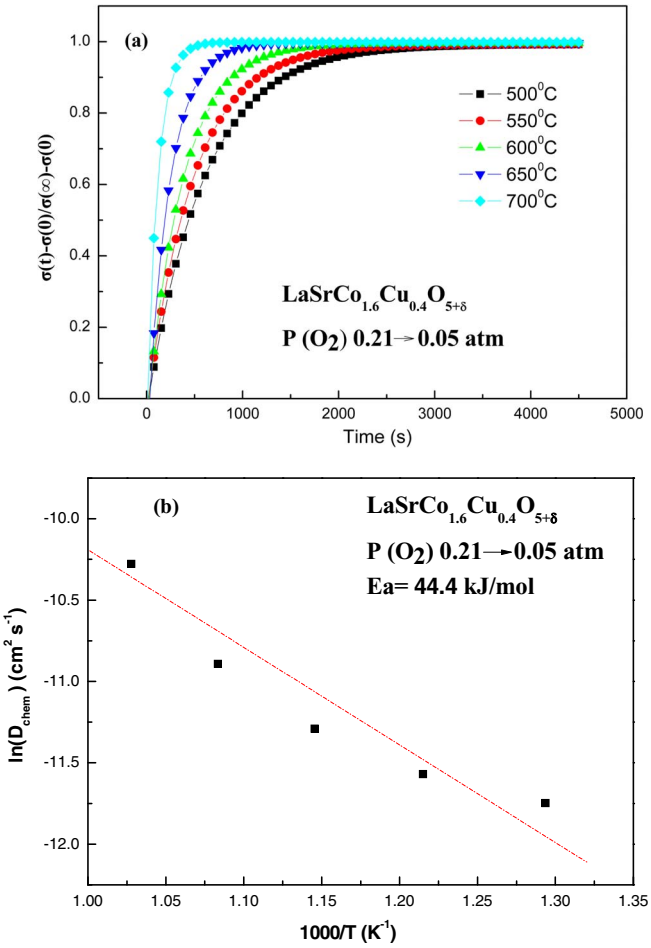

Figure 5. (a) Normalized conductivity relaxation plots for $LaSrCo_{1.6}Cu_{0.4}O_{5+\delta}$ ranged from 500°C to 700°C for reduction step change in oxygen pressure with a final oxygen pressure of 0.05 atm; (b) Arrhenius plots of D_{chem} vs. 1000/T for SBSC cathode between 500 and 700°C.

kinetics properties. In current resaech, the chemical diffusion coefficient (D_{chem}) and chemical bulk diffusion coefficient coefficient (k_{chem}) were measured using the ECR technique based on variations in ambient atmosphere. The abrupt change in oxygen partial pressure of the surrounding atmosphere induces a corresponding change of the charge carrier concentration (oxygen vacancy) due to the local electroneutrality requirement.[47] The relaxation process is accompanied by oxygen exchange at the surface and chemical diffusion in the bulk of the oxide sample.[48] Figure 5a presents the electrical conductivity relaxation curves of LSCO-Cu cathode at various temperatures after a sudden change in the oxygen partial pressure from 0.21 to 0.05 atm. The conductivities reached the steady state values faster at higher temperatures than at lower temperatures, leading to the D_{chem} and k_{chem} values of higher temperatures being larger than at lower temperatures. The D_{chem} values were 7.91×10^{-6}, 1.25×10^{-5}, 3.44×10^{-5} $cm^2\ s^{-1}$, and the k_{chem} values were 1.66×10^{-3}, 2.67×10^{-3}, 8.88×10^{-3} $cm\ s^{-1}$ at 500, 600 and 700°C, respectively. The detailed D_{chem} and k_{chem} values regarding the cathode in the reduction process in the temperature range of 500–700°C (Table III). Obviously, the values of k_{chem} are faster than the ones of D_{chem}. These higher kinetics properties at intermediate temperatures imply that LSCO-Cu is a promising candidate for cathode in the SOFCs. The equation of D_{chem} for LSCO-Cu cathode as a function of reciprocal temperature in the temperature range of 500–700°C is listed as follows.

$$3.44 \times 10^{-5} \exp\left(-\frac{44.4\ kJ\ mol^{-1}}{RT}\right)\left(m^2 s^{-1}\right) \qquad [4]$$

Table III. Chemical diffusion coefficients (D_{chem}) and surface exchange coefficient (k_{chem}) of $LaSrCo_{1.6}Cu_{0.4}O_{5+\delta}$ in the range of 500°C–700°C calculated from electrical conductivity relaxation curves during the oxygen partial pressure suddenly changed from 0.21 to 0.05 atm.

Temperature (°C)	D_{chem} ($cm^2\ s^{-1}$)	k_{chem} ($cm\ s^{-1}$)
500	7.91×10^{-6}	1.66×10^{-3}
550	9.45×10^{-6}	2.05×10^{-3}
600	1.25×10^{-5}	2.67×10^{-3}
650	1.86×10^{-5}	4.41×10^{-3}
700	3.44×10^{-5}	8.88×10^{-3}

The D_{chem} and k_{chem} values of LSCO-Cu cathode measured in this work are of the same order of magnitude as those determined with an ECR method from the literature.[49–52] The D_{chem} and k_{chem} of $La_{0.1}Sr_{0.9}Co_{0.8}Fe_{0.2}O_{3-\delta}$ are 1.85×10^{-5} $cm^2\ s^{-1}$ and 2.42×10^{-4} $cm\ s^{-1}$ at 650°C, respectively.[49] Rosemary reported k_{chem} of $La_{0.6}Sr_{0.4}Co_{0.2}Fe_{0.8}O_{3-\delta}$ was 2.0×10^{-3} $cm\ s^{-1}$ at 800°C with a small reduction step by changing oxygen partial pressure from 100% to 3.3%.[50] The D_{chem} and k_{chem} values are 1.3×10^{-4} $cm^2\ s^{-1}$ and 3.3×10^{-5} $cm\ s^{-1}$ at 600°C for $Ba_{0.6}Sr_{0.4}Co_{0.9}Nb_{0.1}O_{3-\delta}$ with the oxidation process by the sudden change of oxygen partial pressure from 0.05 to 0.21 atm.[51] Chen et al. reported that the D_{chem} values of $Ba_{0.5}Sr_{0.5}Co_{0.8}Fe_{0.2}O_{3-\delta}$ determined by an ECR method are between 2.5×10^{-5} and 3.9×10^{-4} $cm^2\ s^{-1}$ for temperatures between 600 and 800°C with a small reduction step by changing oxygen partial pressure from 0.21 to 0.1 atm.[52] The variance between previous paper and this work is attributed to different procedures with oxidation process or reduction procedure applied during the ECR measurement or the variations among samples from different laboratories. The D_{chem} activation energies obtained from the slopes of the Arrhenius plots (D_{chem} vs. 1000/T) was 44.4 kJ mol^{-1} (Fig. 5b). The activation energy may be considered in terms of the enthalpy of mobility of the defects involved in the gas/solid equilibration for the O_2/LSCO-Cu cathodes system. This behavior results from the effect of the oxygen partial pressure, which is significantly related to the concentration of defects and the extent of interactions between defects and mobility.[53]

The polarization resistances of the cathodes were measured directly from the difference between the high- and low-frequency intercepts on the real axis of the impedance plot.[54] Figure 6a presents the typical impedance spectra of $LaSrCo_{1.6}Cu_{0.4}O_{5+\delta}$ cathode measured in a symmetric configuration using AC impedance spectroscopy under open-circuit conditions at various temperatures in air. The ohmic resistance of the cell (R_Ω) was eliminated in the real axis of the impedance plot to clearly demonstrate the difference in the cathode polarization. The catalytic activity of $LaSrCo_{1.6}Cu_{0.4}O_{5+\delta}$ cathodes, as characterized by the total cathode polarization resistance (R_P), was determined from the size of the impedance loop on the real axis.[55] The R_p values of $LaSrCo_{1.6}Cu_{0.4}O_{5+\delta}$ are 0.60, 0.09, and 0.027 $\Omega\ cm^2$ at 600, 700, and 800°C, respectively. The detailed information regarding R_p values of $LaSrCo_{1.6}Cu_{0.4}O_{5+\delta}$ cathode at various temperatures (Table IV).

The exchange current density (i_0), which corresponds to the intrinsic oxygen reduction reaction (ORR) rate, is an important parameter for investigating ORR mechanisms at the cathode.[56,57] The i_0 value is an important index to evaluate the electrochemical properties of a cathode. It can be obtained from AC impedance measurements (EIS). With this technique, the i_0 values are calculated using the R_p, and Equation 5 is derived from the Bulter-Volmer equation:[58]

$$i_0 = \frac{RT\nu}{nFR_P} \qquad [5]$$

Where, n is the total number of electrons passed in the reaction, ν reflects the number of times the rate-determining step occurs for one

Downloaded on 2015-07-15 to IP 134.208.4.209 address. Redistribution subject to ECS terms of use (see ecsdl.org/site/terms_use) unless CC License in place (see abstract).

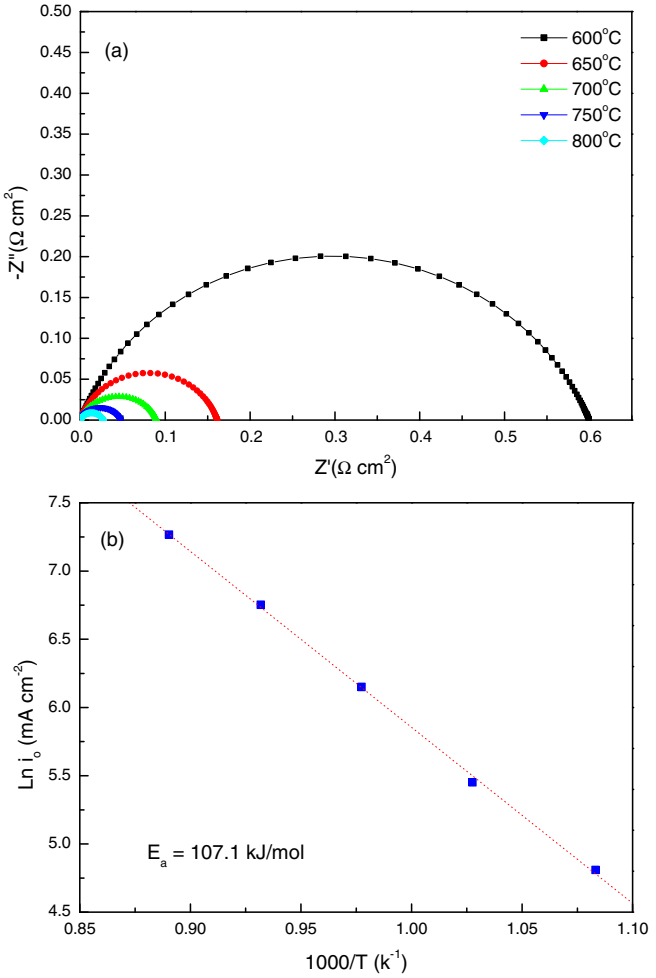

Figure 6. (a) Nyquist diagram of the impedance spectroscopy and (b) Arrhenius plot of Ln (i_0) vs. 1000/T for $LaSrCo_{1.6}Cu_{0.4}O_{5+\delta}$ cathodes on SDC electrolyte ranged over 600–800°C in air, (b).

occurrence of the full reaction, F is Faraday's constant (F = 96500 C mol^{-1}), and R is the ideal gas constant (R = 8.31 J mol^{-1} K^{-1}). For the ORR, n and ν are generally assumed to be 4 and 1, respectively, because the total number of electrons transferred per molecule of oxygen reduced is 4 and the rate-limiting step would likely have a stoichiometry of 1 for the oxygen reduction reaction.[59] The i_0 values of $LaSrCo_{1.6}Cu_{0.4}O_{5+\delta}$ cathode are 120, 1048, and 3302 mA cm^{-2} at 600, 700, and 800°C, respectively (Table III). Figure 6b presents the Arrhenius plots for the i_0 values as a function of the reciprocal of absolute temperature. The linearity of the Arrhenius plots indicates that $LaSrCo_{1.6}Cu_{0.4}O_{5+\delta}$ cathodes are stable as a function of temperature. The overall activation energy for the ORR was determined from the

Table IV. Polarization resistance (R_p) and exchange current density (i_0) for $LaSrCo_{1.6}Cu_{0.4}O_{5+\delta}$ cathode on SDC electrolyte obtained from Nyquist plots at various temperatures.

	$LaSrCo_{1.6}Cu_{0.4}O_{5+\delta}$	
T (°C)	R_P (Ω cm^2)	i_0 (mA cm^{-2})
600°C	0.60	120
650°C	0.16	398
700°C	0.09	1048
750°C	0.047	1836
800°C	0.027	3302

Table V. The peak power densities over the temperature range of 500°C–800°C of the anode-supported single-cells with 0.5M SDC-infiltrated $LaSrCo_{1.6}Cu_{0.4}O_{5+\delta}$ cathode, PLD-deposited SDC/SDC bilayer electrolytes deposited for various time.

	The peak power density (mW cm^{-2})				
T (°C)	0 h	3 h	6 h	9 h	12 h
500°C	253	419	481	324	332
600°C	575	1062	1127	846	712
700°C	790	1218	1190	1084	801
800°C	627	896	705	555	475

slope of the line in the Arrhenius plots (i0 versus 1000/T), using the following equation:

$$\ln i_0 = lnK - \frac{E_a}{RT} \quad [6]$$

Where K is the pre-exponential constant, which can be calculated from the y-intercept, and E_a is the reaction activation energy.[60] The value of E_a for the ORR may be related to several factors such as (1) the different cathode preparation methods; (2) the structure of the cathode; or (3) the different cathode compositions. In this study, the ORR activation energies obtained from the slope of the Arrhenius plots were 107.1 kJ mol^{-1} for $LaSrCo_{1.6}Cu_{0.4}O_{5+\delta}$ cathode.

The dense-SDC layer should be as thin as possible and the layer should be gas impermeable in order to effectively utilize the dense-SDC/SDC bi-layer electrolyte concept to reduce the operating temperature of SOFCs. The dense-SDC layer cannot directly be deposited on anode substrates prepared in this manner since it requires a relatively thick dense-SDC layer to achieve the required gas tightness. This layer reduces the gas leakage of the anode substrate significantly and provides smoother surface for the deposition of the dense-SDC layer due to the nanostructural nature of the PLD films.[8] An anode-supported single fuel cell with a dense PLD-deposited SDC layer, a SDC electrolyte (30 μm), a Ni-SDC anode (1mm), and a LSCO-Cu cathode (20 μm) was fabricated to evaluate the performance of the single cell,. The performance (including I-V curve and I-P curve under different operating temperatures) of the LSCO-Cu cathode infiltrated with 0.5M SDC in anode-supported SOFCs using PLD-deposited SDC/SDC as bilayer electrolytes for various PLD deposition time (Fig. 7). Obviously, the single cells with PLD-deposited SDC layer with better performance compared than the single cell without PLD-deposited SDC layer. The maximum peak power densities were located at operating temperature of 700°C for all specimens. Generally, the thickness of PLD-deposited SDC layer is proportional to the deposition time. In this study, the maximum peak power densities are 1218 mW cm^{-2} at operating temperature of 700°C for 3 h PLD-deposition-time. Table V summarizes the peak power densities of the LSCO-Cu cathodes deposited dense SDC layer via PLD for various time over the temperature range of 500°C–800°C. We speculated that the SDC layer is not dense enough for a deposition time less than 3 h; whereas the SDC layer is too thick to reduce the performance of the single cells for a deposition time greater than 9 h. The proper PLD deposition time is about 3–6 h that the single cells have shown good peak power densities. The single cells with high peak power densities come from two main reason: (1) the dense SDC layer prepared via PLD technique as a blocking layer improved the stability of the SDC electrolyte under the reducing environment and inhibit electronic current leakage and inhibited electronic current leakage, and (2) the infiltration the SDC electrolyte nanoparticles into the porous LSCO-Cu cathode backbones really improve the electrochemical performance. The newly formed electrolyte of SDC nanopowders deposited on the LSCO-Cu cathode with porous skeleton would allow gas-phase molecules to easily diffuse to the SDC/LSCO-Cu boundaries where the sites took place ORR.

Downloaded on 2015-07-15 to IP 134.208.4.209 address. Redistribution subject to ECS terms of use (see ecsdl.org/site/terms_use) unless CC License in place (see abstract).

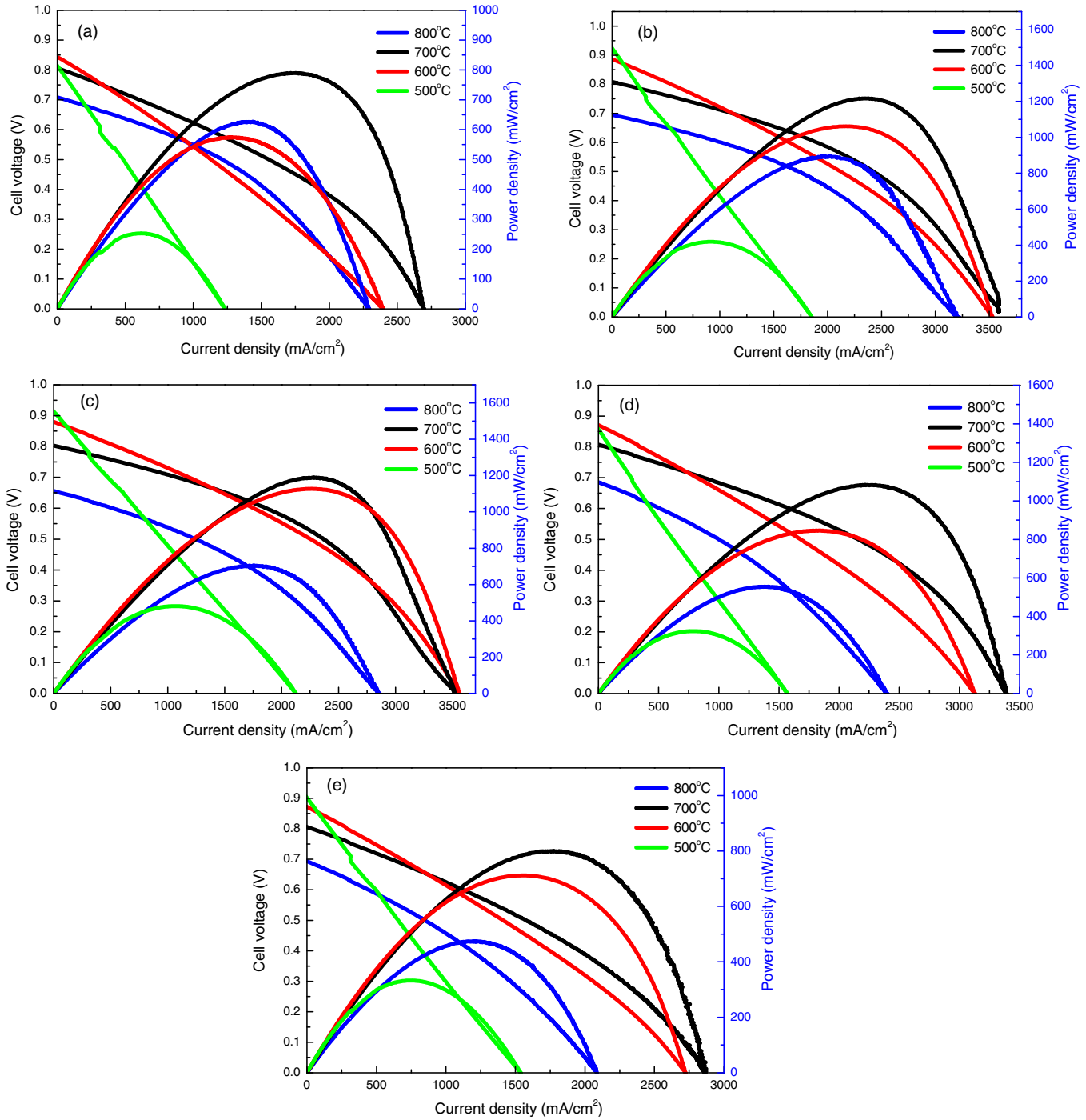

Figure 7. The I-V and I-P curve for NiO+SDC/SDC/LSCO-Cu single cell deposited dense SDC layer as bilayer electrolytes for (a) 0 h, (b) 3 h, (c) 6 h, (d) 9 h and (e) 12 h measured over 500–800°C; where $LaSrCo_{1.6}Cu_{0.4}O_{5+\delta}$ cathode infiltrated with 3 μL of 0.5 M SDC.

Conclusions

In this study, the oxygen bulk diffusion properties and electrochemical properties of LSCO-Cu cathode was investigated. The D_{chem} equation as a function of reciprocal temperature in the temperature range of 500–700°C is listed as follows.

$$3.44 \times 10^{-5} \exp\left(-\frac{44.4\ kJ\ mol^{-1}}{RT}\right)\left(m^2 s^{-1}\right)$$

Moreover, using a pulsed laser technique (PLD) deposited a dense $Ce_{0.8}Sm_{0.2}O_{1.9}$ (SDC) thin layer on thick SDC as bi-layer electrolyte and infiltrating SDC nanoparticles onto LSCO-Cu skeleton to improve the performance of a single cell. An anode-supported single cell with PLD-deposited SDC/SDC bilayer, 0.5 M SDC-infiltrated $LaSrCo_{1.6}Cu_{0.4}O_{5-\delta}$ cathode exhibits good performance at low operating temperatures. The cell reaches power densities of 1062 mW cm^{-2} at 600°C, 1218 mW cm^{-2} at 700°C for 3 h PLD-deposition-time, and 1127 mW cm^{-2} at 600°C, 1190 mW cm^{-2} at 700°C for 6 h PLD-deposition-time. The significant increase in electrochemical performances was mainly attributed to the creation of extra electrolyte/cathode phase boundaries by infiltration method and the reduction of electrical current

Downloaded on 2015-07-15 to IP 134.208.4.209 address. Redistribution subject to ECS terms of use (see ecsdl.org/site/terms_use) unless CC License in place (see abstract).

leakage in the single cell by PLD-deposited SDC/SDC bilayer electrolyte.

Acknowledgments

The authors thank the National Science Council of Taiwan for financially supporting this research under contract number: MOST 103-2113-M-259-002 and MOST 103-2120-M-259-001.

References

1. D. Chen, G. Yang, Z. Shao, and F. Ciucci, *Electrochem. Commun.*, **35**, 131 (2013).
2. T. Hong, L. Zhang, F. Chen, and C. Xia, *J. Power Sources*, **218**, 254 (2012).
3. J. J. Choi, K. S. Cho, J. H. Choi, J. Ryu, B. D. Hahn, W. H. Yoon, J. W. Kim, C. W. Ahn, D. S. Park, and J. Yun, *Int. J. Hydrogen Energy*, **37**, 6830 (2012).
4. H. Uchida, S. Arisaka, and M. Watanabe, *Electrochem. Solid-State Lett.*, **2**, 428 (1999).
5. M. Camaratta and E. Wachsman, *J. Electrochem. Soc.*, **155**, B135 (2008).
6. F. Bozza, R. Polini, and E. Traversa, *Fuel Cells*, **8**, 344 (2008).
7. T. Shimonosono, Y. Hirata, Y. Ehira, S. Sameshima, T. Horita, and H. Yokokawa, *Solid State Ionics*, **174**, 27 (2004).
8. Q. L. Liu, K. A. Khor, S. H. Chan, and X. J. Chen, *J. Power Sources*, **162**, 1036 (2006).
9. A. Atkinson, *Solid State Ionics*, **95**, 249 (1997).
10. S. P. S. Badwal, F. T. Ciacchi, and J. Drennan, *Solid State Ionics*, **121**, 253 (1999).
11. L. Zhang, C. Xia, F. Zhao, and F. Chen, *Mater. Res. Bull.*, **45**, 603 (2010).
12. D. Yang, X. Zhang, S. Nikumb, C. Deces-Petit, R. Hui, R. Maric, and D. Ghosh, *J. Power Sources*, **164**, 182 (2007).
13. J. H. Joo and G. M. Choi, *Solid State Ionics*, **177**, 1053 (2006).
14. D. Pergolesi, E. Fabbri, and E. Traversa, *Electrochem. Commun.*, **12**, 977 (2010).
15. P. N. Dyer, R. E. Richards, S. L. Russck, and D. M. Taylor, *Solid State Ionics*, **134**, 21 (2000).
16. J. P. P. Huijsmans, F. P. F. Van Berkel, and G. M. Christie, *J. Power Sources*, **71**, 107 (1998).
17. B. C. H. Steele, K. M. Hori, and S. Uchino, *Solid State Ionics*, **135**, 445 (2000).
18. Z. P. Shao and S. M. Haile, *Nature*, **431**, 170 (2004).
19. W. Zhou, Z. P. Shao, R. Ran, W. Q. Jin, and N. P. Xu, *Chem. Commun.*, **44**, 5791 (2008).
20. A. Egger, E. Bucher, M. Yang, and W. Sitte, *Solid State Ionics*, **225**, 55 (2012).
21. A. Chroneos, B. Yildiz, A. Tarancon, D. Parfitt, and J. A. Kilner, *Energy Environ. Sci.*, **4**, 2774 (2011).
22. J. Xue, Y. Shen, and T. He, *Int. J. Hydrogen Energy*, **36**, 6894 (2012).
23. A. Tarancón, S. J. Skinner, R. J. Chater, F. Hernández-Ramírez, and J. A. Kilner, *J. Mater. Chem.*, **17**, 3175 (2007).
24. A. A. Taskin, A. N. Lavrov, and Y. Ando, *Phys. Rev. B*, **71**, 134414 (2005).
25. A. A. Taskin, A. N. Lavrov, and Y. Ando, *Appl. Phys. Lett.*, **86**, 091910 (2005).
26. Q. Ma, R. Peng, Y. Lin, J. Gao, and G. Meng, *J. Power Sources*, **161**, 95 (2006).
27. T. Hibino, A. Hashimoto, M. Suzuki, and M. Sano, *J. Electrochem. Soc.*, **149**, A1503 (2002).
28. Y. Huang, J. Vohs, and R. Gorte, *J. Electrochem. Soc.*, **151**, A646 (2004).
29. H. Ding and X. Xue, *Electrochimica Acta*, **55**, 3812 (2010).
30. D. Chen and Z. Shao, *Int. J. Hydrogen Energy*, **36**, 6948 (2011).
31. E. Bucher, A. Egger, P. Ried, W. Sitte, and P. Holtappels, *Solid State Ionics*, **179**, 1032 (2008).
32. X. Chen, S. Wang, Y. L. Yang, L. Smith, N. J. Wu, B. I. Kim, S. S. Perry, A. J. Jacobson, and A. Ignatievet, *Solid State Ionics*, **146**, 405 (2002).
33. A. Zomorrodian, H. Salamati, Z. G. Lu, X. Chen, N. J. Wu, and A. Ignatiev, *Int. J. Hydrogen Energy*, **35**, 12443 (2010).
34. I. Yasuda and M. Hishinuma, *J. Solid State Chem.*, **123**, 382 (1996).
35. J. M. Vohs and R. J. Gorte, *Adv. Mater.*, **21**, 943 (2009).
36. R. Kiebach, C. Knöfel, F. Bozza, T. Klemensø, and C. Chatzichristodoulou, *J. Power Sources*, **228**, 170 (2013).
37. T. Klemensø, C. Chatzichristodoulou, J. Nielsen, F. Bozza, K. Thydén, R. Kiebach, and S. Ramousse, *Solid State Ionics*, **224**, 21 (2012).
38. Z. Liu, D. Ding, B. Liu, W. Guo, W. Wang, and C. Xia, *J. Power. Sources*, **196** 8561 (2011).
39. Y. P. Fu and M. Y. Hsieh, *J. Am. Ceram. Soc.*, **97**, 3230 (2014).
40. Y P. . Fu, S. B. Wen, and C. H. Lu, *J. Am. Ceram. Soc.*, **91**, 127 (2008).
41. C. Huang, D. Chen, Y. Lin, R. Ran, and Z. Shao, *J. Power Sources*, **195**, 5176 (2010).
42. K. Huang, H. Y. Lee, and J. B. Goodenough, *J. Electrochem. Soc.*, **145**, 3220 (1998).
43. M. A. Senaris-Rodriguez and J. B. Goodenough, *J. Solid State Chem.*, **116**, 224 (1995).
44. A. Jun, J. Shin, and G. Kim, *Phys. Chem. Chem. Phys.*, **15**, 19906 (2013).
45. Y. P. Fu, C. H. Li, J. Ouyang, S. H. Hu, and K. W. Tay, *J. Electrochem. Soc.*, **159**, F426 (2012).
46. L. W. Tai, M. M. Nasrallah, H. U. Anderson, D. M. Sparlin, and S. R. Sehlin, *Solid State Ionics*, **76**, 259 (1995).
47. H. Dunwald and C. Wagner, *Z. Phys. Chem. B*, **24**, 53 (1934).
48. J. E. Elshof, M. H. R. Lankhorst, and H. J. M. Bouwmeester, *J. Electrochem. Soc.*, **144**, 1060 (1997).
49. M.-B. Choi, K.-T. Lee, H.-S. Yoon, S.-Y. Jeon, E. D. Wachsman, and S.-J. Song, *J. Power Sources*, **220**, 377 (2012).
50. R. A. Cox-Galhotra and S. McIntosh, *Solid State Ionics*, **181**, 1429 (2010).
51. C. Huang, D. Chen, Y. Lin, R. Ran, and Z. Shao, *J. Power Sources*, **195**, 5176 (2010).
52. D. Chen and Z. Shao, *Int. J. Hydrogen Energy*, **36**, 6948 (2011).
53. T. Bak, J. Nowotny, and C. C. Sorrel, *J. Phys. Chem. Solids*, **65**, 1229 (2004).
54. Y. Leng, S. H. Chan, and Q. Liu, *Int. J. Hydrogen Energy*, **33**, 3808 (2008).
55. L. Nie, M. Liu, Y. Zhang, and M. Liu, *J. Power Sources*, **195**, 4704 (2010).
56. M. Kleitz and F. Petitbon, *Solid States Ionics*, **92**, 65 (1996).
57. A. Ringuede and J. Fouletier, *Solid States Ionics*, **139**, 167 (2001).
58. J. Piao, K. Sun, N. Zhang, X. Chen, S. Xu, and D. Zhou, *J. Power Sources*, **172**, 633 (2007).
59. J. Liu, A. C. Co, B. Paulson, and V. I. Briss, *Solid State Ionics*, **177**, 377 (2006).
60. A. C. Co, S. J. Xia, and V. I. Briss, *J. Electrochem. Soc.*, **152**, A570 (2005).

Downloaded on 2015-07-15 to IP 134.208.4.209 address. Redistribution subject to ECS terms of use (see ecsdl.org/site/terms_use) unless CC License in place (see abstract).

View publication stats